Materials Today Bio 16 (2022) 100420

Contents lists available at ScienceDirect

Materials Today Bio

journal homepage: www.journals.elsevier.com/materials-today-bio

Iron corroded granules inhibiting vascular smooth muscle cell proliferation☆

Dongxu Qiu [a], Yalan Deng [b], Yanbin Wen [a], Jun Yin [a], Jie Feng [a], Jiabing Huang [c], Mingyu Song [a], Gui Zhang [d], Changqing Chen [a,**], Jian Xia [a,*]

[a] Department of Neurology, Xiangya Hospital, Central South University, Changsha, Hunan, 410008, PR China
[b] NHC Key Laboratory of Cancer Proteomics & Laboratory of Structural Biology, Xiangya Hospital, Central South University, Changsha, 410008, Hunan, PR China
[c] Department of Cardiology, The Second Affiliated Hospital of Nanchang University, Jiangxi, Nanchang, PR China
[d] R&D Center, Lifetech Scientific (Shenzhen) Co Ltd, Shenzhen, 518057, PR China

ARTICLE INFO

Keywords:
Vascular smooth muscle cell
Proliferation
Iron-based stent
Corroded granules
Neointimal hyperplasia
In-stent restenosis

ABSTRACT

In-stent restenosis after interventional therapy remains a severe clinical complication. Current evidence indicates that neointimal hyperplasia induced by vascular smooth muscle cell (VSMC) proliferation is a major cause of restenosis. Thus, inhibiting VSMC proliferation is critical for preventing in-stent restenosis. The incidence of restenosis was reduced in nitrided iron-based stents (hereafter referred to as iron stents). We hypothesized that the corroded granules produced by the iron stent would prevent in-stent restenosis by inhibiting VSMC proliferation. To verify this hypothesis, we introduced a dynamic circulation device to analyze the components of corroded granules. To investigate the effects of corroded granules on VSMC proliferation, we implanted the corroded iron stent into the artery of the atherosclerotic artery stenosis model. Moreover, we explored the mechanism underlying the inhibition of VSMC proliferation by iron corroded granules. The results indicated that iron stent produced the corroded granules after implantation, and the main component of the corrosion granules was iron oxide. Remarkably, the corroded granules reduced the neointimal hyperplasia in an atherosclerotic artery stenosis model, and iron corroded granules decreased the neointimal hyperplasia by inhibiting VSMC proliferation. In addition, we revealed that corroded granules reduced VSMC proliferation by activating autophagy through the AMPK/mTOR signaling pathway. Importantly, safety of iron corroded granules was evaluated and proved to be satisfactory hemocompatibility in rabbit model. Overall, the role of corroded granules in restenosis prevention was described for the first time. This finding highlighted the implication of corroded granules produced by iron stent in inhibiting VSMC proliferation, pointing to a new direction to prevent in-stent restenosis.

1. Introduction

Vascular smooth muscle cells (VSMC) are the predominant cell type in the medial layer of vessel walls. VSMCs exhibited high contractility and low proliferation rates under physiological conditions [1–3]. However, they are not terminally differentiated and can switch to synthetic phenotypes under certain conditions (e.g., vessel wall injury). The synthetic phenotype of VSMC was characterized by the loss of contractility, high proliferation rate, and increased motility, which contributed to neointimal hyperplasia after stenting [4,5]. Drugs such as paclitaxel and rapamycin, when coated on the stent surface, inhibited intimal hyperplasia by suppressing VSMC [6,7]. However, in addition to inhibiting VSMC, the neo-endothelial formation was also delayed, as the anti-proliferative effects were not specific to VSMC [8,9]. Therefore, stents that specifically target VSMCs are the next revolution in interventional technologies.

Bioresorbable stents were heralded as the fourth revolution in interventional technology and were designed to avoid the long-term health risks posed by drug-eluting stents (DES) [10,11]. Iron has demonstrated excellent biocompatibility and mechanical performance [12–14]. In

☆ Dongxu Qiu and Yalan Deng contributed equally to this study.

* Corresponding author.
** Corresponding author.
E-mail addresses: qiudongxu1988@csu.edu.cn (D. Qiu), dyl1881010@csu.edu.cn (Y. Deng), 13873117882@163.com (C. Chen), xjian1216@csu.edu.cn (J. Xia).

https://doi.org/10.1016/j.mtbio.2022.100420
Received 2 July 2022; Received in revised form 1 September 2022; Accepted 3 September 2022
Available online 6 September 2022

addition, iron is an essential element involved in diverse physiological processes, including DNA synthesis and oxygen binding [15–17]. Moreover, iron played a beneficial role by antagonizing VSMC proliferation. By introducing the cell culture model at phenotypic and molecular level, Mueller et al. observed that iron inhibit VSMC proliferation by regulating the genes that requiring for cell proliferation, cell cycle progression or DNA replication [18]. Moreover, by co-culture with iron particles, the viability of VSMC was dose-dependently affected due to the up-regulation of oxidative stress gene heme oxygenase-1 [19,20]. It also indicated that iron particles arrested VSMC in the G0/G1 phase by inducing the generation of hydroxyl radicals [21–23]. However, this beneficial effect has only been demonstrated *in vitro* and warrants *in vivo*

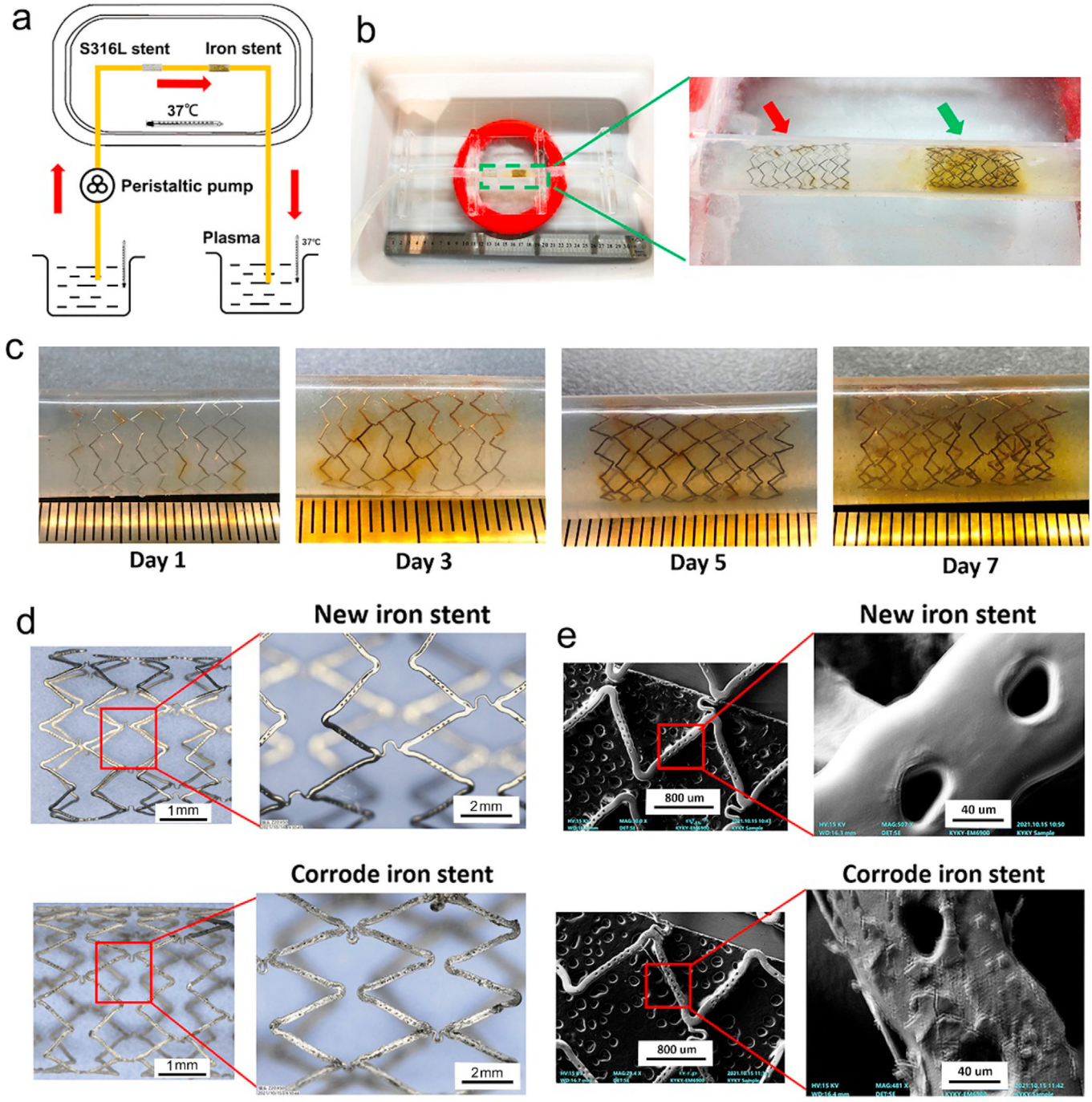

Fig. 1. Dynamic circulation device and corroded granules produced by iron stent. (a) Schematic of circulation model: a peristaltic pump was applied to mimic vessel pulsation, the silastic tube was connected to the peristaltic pump, and the pump transferred plasma from one end to the other. (b) To mimic the corroded microenvironment of the vessel, agarose was used to cover the iron stent. The stainless-steel stent (S316L) was set as the control. Red and green arrows indicate the S316L stent and iron stent, respectively. (c) Localized corrosion could be observed in iron stent after 3 days' dynamic circulation test. The stent turned reddish brown. Uniform corrosion was exhibited on surfaces of the iron stent after 7 days' dynamic circulation test, and insoluble yellow corroded granules were observed around the struts. (d–e) Pitting corrosion was extensively generated in iron stent, and the surface became rough and uneven. (f) The components of the corroded iron stent were detected to be much more complex than those of the new iron stent. The element ratio changed in corroded granules (e.g., element ratios, including O and C, increased, whereas the ratio of Fe and P decreased). (For interpretation of the references to colour in this figure legend, the reader is referred to the Web version of this article.)

validation. The incidence of intimal hyperplasia was lower in iron stents than in S316L stainless-steel stents [12,24]. The production of corroded iron granules was the major difference between the two stents. Therefore, corroded granules were assumed to prevent restenosis by inhibiting VSMC proliferation. To verify this hypothesis, we implanted a corroded iron stent in the carotid artery. Iron-corroded granules were found to inhibit VSMC proliferation by activating autophagy through the AMPK/mTOR signaling pathway, which prevents restenosis after iron stent implantation. Notably, we also found that the corroded granules were hemocompatible. Overall, this study highlights the role of iron-corroded granules in VSMC proliferation and provides a new framework for restenosis prevention after stenting.

2. Materila and methods

2.1. Stent parameters and performance

The microstructure and composition of nitrided iron-based (Fe alloyed with 0.074 wt% N) stent were presented in a previous study [25]. The nitrided iron used in this study was Fe alloyed with 0.074 wt% N, struts thickness: 70 μm, Φ:3.0 × 18 mm. The S316L stent had the same design as the nitrided iron stent, and the parameters of the S316L stent were as follows: strut thickness, 70 μm; Φ, 3.0 × 18 mm. Iron and S316L were manufactured by Lifetech Scientific Co. Ltd. (Shenzhen, China). Vacuum plasma nitrided at 50 Pa (N_2:H_2 = 1:3) at 500 °C for 2 h was applied to produce the nitrided iron stent. All nitrided iron stents/S316L stent were electrochemically polished and crimped into the balloon of a rapid exchange catheter using an automatic crimping machine. All devices underwent the final ethylene oxide sterilization process.

2.2. Corroded granules produced by iron stent

As presented in Fig. 1a–b, the device used in this experiment consisted of three different parts: agarose covering the stent setup, the monitoring machine, and the pumping system. The device workflow is as follows. First, one end of the silastic tube was firmly connected to the recycling pump, whereas the other end was immersed in Hank's solution. The pump was used to transfer Hank's solution from one end to the other, and a monitor machine was connected to the conduit system. This monitoring machine was used to record changes in parameters such as pH, Hank's solution temperature, and the dynamic velocity of the flow. Hank's solution temperature was set between 36 °C and 37 °C, and the pH was set between 7.35 and 7.45. The flow field parameters of peristaltic pump are presented as following: Hank's solution in reservoir was circulated at a constant rate of 550 ml/min. To calculate the corrosion rate of the iron stent, the initial mass of iron stents was recorded prior experiment. Agarose was used to cover the iron stent to mimic the corroded microenvironment of the vessels. The S316L stent was used as a control. All the stents were placed in the middle of the conduit. The stent appearance and corrosion pits were monitored during system operation. Different time points, including 24, 36, and 72 h, were used to evaluate changes to the stent.

2.3. Iron corroded granules collection

Iron-based stent and S316L stent were cut into 0.1 × 0.1 mm pieces. Then those granules were stored in a desiccator for 24 h and sterilized by exposure to ultraviolet irradiation. After the sterilized process, the dynamic corrosion bench was applied. The pH value (7.35–7.45), temperature (37 ± 0.5 °C), and dissolved oxygen (2.8–3.2 mg) of this device were well controlled to approach the common values in human artery. Modified HyCloneTM Hanks' Balanced Salt Solution was used for the corrosive media as its ionic composition is similar to that of blood plasma. The granules were immersed into the HyCloneTM Hanks' Balanced Salt Solution for 7 days. After the corrosion procedure, the corrosion granules were taken out, and then rapidly dried by the cool air from a blower.

2.4. RNA isolation and real-time PCR

An RNeasy Mini Kit (Qiagen) was used to collect cellular RNA following the manufacturer's instructions. A TaqMan reverse transcription kit (Applied Biosystems) was used for reverse transcription following the manufacturer's instructions. The iQTM SYBR Green Supermix (Bio-Rad) was used for amplification. The comparative Ct method was used to determine relative mRNA quantities. The process was normalized to glyceraldehyde-3-phosphate dehydrogenase (GAPDH). GAPDH forward primer, 5′-ACAGCAACAGGGTGGTGGAC-3′ and reverse primer, 5′-TTTGAGGGTGCAGCGAACTT-3′.

2.5. Stent implantation

All the rabbits received 10 mg aspirin and 10 mg clopidogrel the day before the surgery. Before anesthesia and mechanical ventilation, the rabbits were subcutaneously injected with diazepam (1 mg/kg) and ketamine (25 mg/kg). The right femoral artery was surgically exposed and a 4 F guide catheter was introduced using a 0.014-inch guidewire. A stent/stent was introduced and positioned on the right side of the carotid artery. The balloon catheters were inflated to 7–9 atm for 30s to deploy the stent/stent. The parameters of the stent/stent have been described in section 2.1. To avoid clotting during surgery, heparin (200 IU/kg) was administered via catheter to maintain an activated coagulation time of >300 s. All animals were fed a normal diet produced by the Guangzhou Feed Institute. A minimum of six animals were used in each experimental group. The initial mass of the stent was recorded before implantation. All experimental procedures were approved by the Institutional Animal Ethics Committee of Xiangya Hospital.

2.6. Carotid artery angiography detection

Angiographic images of the carotid artery were obtained using the CGO-2100 Cath-Lab system (Wandong, China). Briefly, an angiographic catheter was introduced at the proximal end of the carotid artery, and a contrast agent was injected into the artery through the angiographic catheter. Thereafter, the CGO-2100 Cath-Lab system was used to obtain X-ray images of the same artery location, both before and after injecting the contrast agent. The images were subtracted using the system to obtain results. The protocol and procedures employed were reviewed and approved by the appropriate institutional review committee.

2.7. Transmission electron microscopy (TEM)

VSMCs were collected to detect autophagosomes using TEM (H7500, Hitachi). Pretreated samples were fixed in 2.5% glutaraldehyde in 0.1 M PBS buffer and 1% osmium tetroxide (OsO_4). The samples were then dehydrated in alcohol and infiltrated with Araldite-Epon. TEM was used to capture the autophagosomes in the samples. Each sample was analyzed more than thrice.

2.8. Statistical analysis

The SPSS software package (version 18.0; SPSS Inc. Chicago. USA) was used for statistical analysis. One-way analysis of variance (ANOVA) was used to assess statistical differences between groups. Statistical significance was set at $P < 0.05$.

3. Results

3.1. Detailed observation of corroded granules produced by iron stent

To detect the corroded granules produced by the iron stent, a peristaltic pump was used to mimic the pulsation of the vascular artery, as shown in Fig. 1a–b. The iron stent showed no conspicuous changes on the surface after 1 day of the dynamic circulation test. Notably, localized

corrosion was observed in the iron stent after 3 days' circulation test, and the stent appeared reddish brown. When the iron stent was corroded for seven days, uniform corrosion was observed on the surfaces of the iron stent, and yellow insoluble corroded granules were observed around the struts (Fig. 1c). In particular, pitting corrosion was generated extensively in the iron stent, the corrosion morphology of iron stent was exhibited in Fig. 1d–e. The surface of the corroded iron stent become rough and uneven, with large cracked shell-shaped corrosion products generated and distributed throughout the surface. The weight of iron stent was reduced by 2.1 ± 0.6, 6.2 ± 1.9, and 14.1 ± 2.2 mg at 24, 48, and 72 h after the circulation test. The average corrosion rate was 0.38 ± 0.08 mm/year. X-ray diffraction (XRD) was performed to identify the components of iron corroded granules further. According to the XRD analysis, major peaks were attributed to the iron matrix. In addition, weak peaks of iron oxide were found in the 2θ range of 30–70°. The characteristic peaks at 2θ = 32.9°, 33.5° and 36.2° were also found by diffraction patterns, corresponding to the (100–0), (0002) and (100–1) planes of the crystal, respectively.

3.2. VSMC proliferation was inhibited by implanting the corroded iron stent

To detect the effects of corroded granules on VSMC proliferation, we implanted the corroded iron stent into the carotid artery in a rabbit model, and the S316L stent was used as the control (Fig. 2a–d). All rabbits (n = 12; weight 5.0 kg ± 0.4 kg) were successfully stented, and no peri-procedural complications occurred during the experiment period. Month 6 was set as the time point to evaluate the results. All rabbits remained healthy until the final follow up. HE staining showed that the intimal thickness was much lower in the corroded iron stent-implanted group (Fig. 2e–f), and the intima/media (I/M) ratio was also decreased. The proliferation of VSMC was assessed using flow cytometry, and the results indicated that the percentage of VSMC in the S phase was reduced in the corroded iron stent group. However, no differences were detected in the G0/G1 and G2/M phases (Fig. 2g–h). To investigate the inhibition of VSMC proliferation further, osteopontin (OPN) expression was detected using IF staining. Its expression was reduced in the corroded iron stent group (Figs. S1a–b). Moreover, we measured α-SMA expression in both groups. Consistent with the OPN results, the expression of α-SMA also decreased in the intima layer in the corroded iron stent-implanted group (Figs. S1c–d). S100A4 demonstrated to be the reliable marker of synthetic phenotype VSMCs by inhibiting phosphorylation of target proteins. Then we measured the expression of S100A4 between corroded iron stent group and the control. The expression of S100A4 was decreased in corroded iron stent group (Fig. S4h).

Because corroded granules are produced several days after stent implantation, VSMC should not be affected following implantation of the iron stent in the initial period. Based on this fact, we evaluated VSMC proliferation at both month 1 and month 6 after stent implantation. As expected, a few corroded granules were detected on month 1, whereas numerous corroded granules were observed on month 6 (Fig. 2i). In accordance with the deposition of corroded granules, the expression of both OPN and α-SMA decreased on month 6 (Fig. 2j–k). Collectively, these findings are consistent with the results drawn above, further confirming that corroded granules play an important role in VSMC proliferation.

3.3. Corroded granules inhibit VSMC proliferation in vitro

To further investigate the effects of corroded granules on VSMC proliferation, we performed a co-culture experiment. As shown in Fig. 3a–b, more VSMCs were observed on the surface of the S316L stent than on the corroded iron stent after 72 h. VSMC proliferation was detected using the EdU assay. Consist with the results of the co-culture assay, there were three-fold fewer EdU-positive cells detected in the group pretreated with corroded iron granules (Fig. 3c). In addition, flow cytometry was conducted to measure VSMC proliferation. The percentage of VSMC was markedly decreased in the S phase in the corroded iron granule group (Fig. 3d–e). Moreover, corroded granules attenuated VSMC proliferation in a dose-dependent manner (the optimal concentration was about 10 mg/L) (Fig. 3f–g). In addition to VSMC proliferation, VSMC migration also proved to be associated with neointima formation after stenting. Thus, scratch-wound assays were performed to determine the role of corroded granules in this process. However, no statistically difference was yield of the VSMC migration when pretreated with the corroded iron granules. Similar results were obtained in transwell migration assay (data not shown). Those data suggested that iron corroded granules inhibit VSMC proliferation but not migration *in vitro*. Moreover, the co-culture experiment was performed to explore the effects of iron corroded granules on endothelial cell further. As presented in Figs. S4a–b, no statistic differences were detected in the number of HUVECs. CCK-8 assay revealed the absorbance value at 450 nm were almost the same between the two groups (Fig. S4c).

3.4. Corroded iron granules inhibited VSMC proliferation by activating autophagy

Autophagy has been shown to inhibit VSMC proliferation to prevent neointimal hyperplasia. VSMCs were restrained after the corroded granules were produced. Thus, we determined whether the corroded granules regulate autophagy in VSMC after the iron stent was implanted. Western blotting showed that the expression of p62 protein and LC3-II, which are biomarkers of autophagy, was higher in the corroded iron stent group than in the S316L stent implanted group (Figs. S2a–c). Moreover, using transmission electron microscopy, we found that the formation of autophagosomes was markedly increased in the iron stent group (Figs. S2d–e). To further clarify whether the corroded granules induced autophagy in PDGF-treated VSMC *in vitro*, we conducted co-culture experiments; p62 and LC3-II were remarkably upregulated in the corroded granule group. However, the effect vanished after pretreatment with the autophagy inhibitor 3-MA (Figs. S2f–g). To investigate whether the corroded granules inhibited VSMC proliferation by activating autophagy, we performed an EdU assay in the study. The number of EdU-positive cells in the corroded granules group were much fewer than that in the stainless granules group. However, this effect was eliminated after pretreatment with 3-MA (Fig. S2h). Consistent with the EdU test, the CCK-8 assay also indicated that the corroded iron granules remarkably reduced cell viability in PDGF-stimulated VSMC, but this effect was attenuated after co-treatment with 3-MA (Fig. S2i).

3.5. Corroded granules induced autophagy through AMPK/mTOR signaling pathway

Activation of the AMPK/mTOR pathway induces autophagy was reported to restrain VSMC proliferation in balloon-injured arteries. Thus, we speculated that the corroded granules induced autophagy by activating the AMPK/mTOR signaling pathway. To test this hypothesis, we measured the expression of AMPK/mTOR-related proteins *in vitro*. Western blotting showed that the phosphorylation of AMPK (p-AMPK) and the protein level of LC3-II were increased in the pre-treated group, whereas the phosphorylation of mTOR (p-mTOR) was reduced (Fig. 4a–c). To confirm the role of AMPK activity in autophagy regulated by corroded granules, we performed si-AMPK transfection experiments. LC3-II and p62 expression was induced by corroded granules decreased in AMPK-deficient VSMC (Fig. 4d). Additionally, the number of EdU-positive cells was remarkably increased in AMPK-deficient VSMC (Fig. 4e–f). To further address the role of mTOR in autophagy, we introduced the specific autophagy inducer rapamycin, which inhibits the mammalian target of rapamycin (mTOR) pathway by binding to mTORC1. After rapamycin inhibited the mTOR pathway, the decreased protein expression of p62 and LC3-II were elevated in the negative control group (Fig. 4g). Rapamycin pretreatment significantly reduced

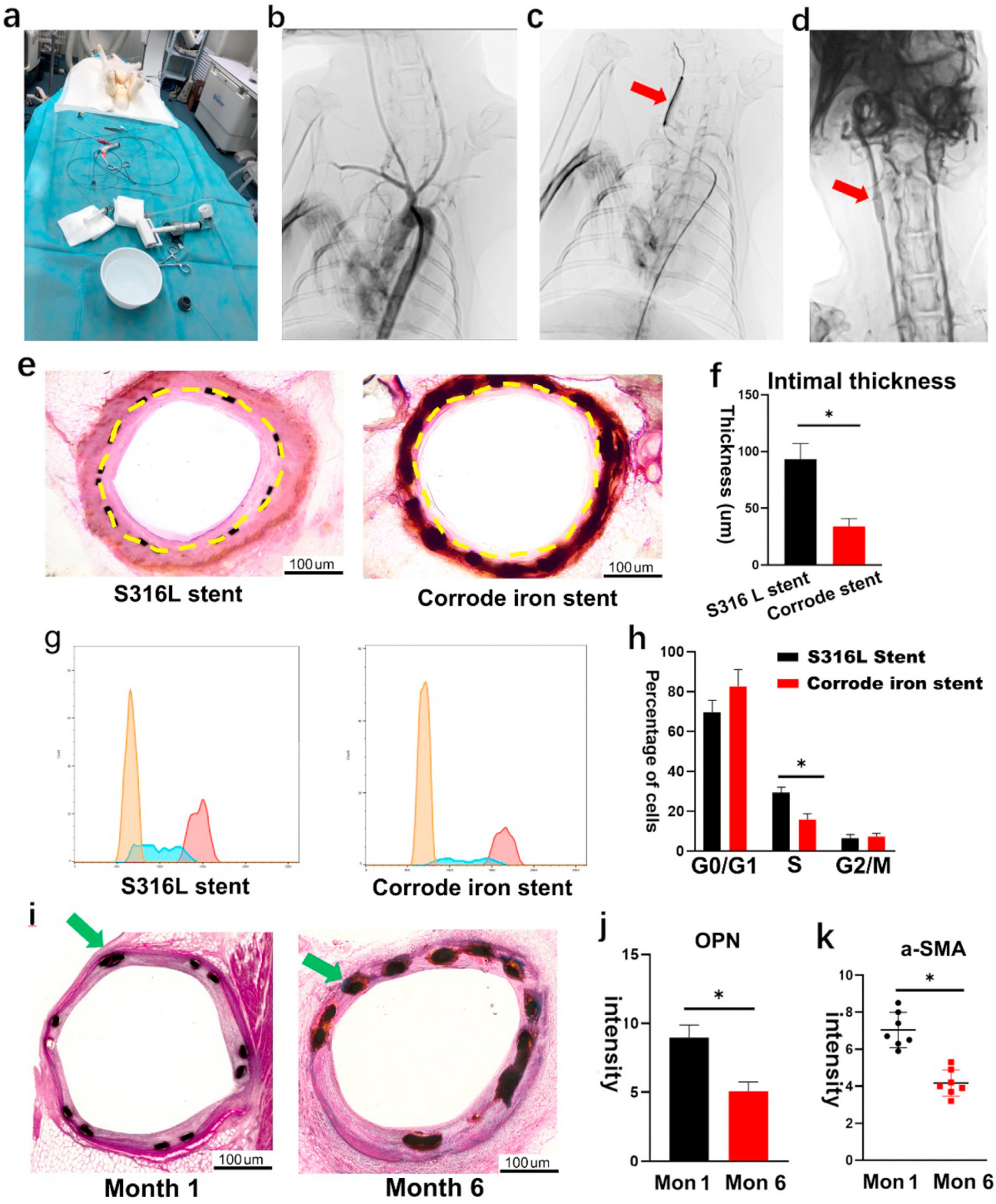

Fig. 2. VSMC proliferation was inhibited by implanting the corroded iron stent. (a) Stent implantation surgery in rabbits. The right femoral artery was surgically exposed, and a 4 F guide catheter was introduced with guidewire. All rabbits (n = 12; weight 5.0 kg ± 0.4 kg) were successfully stented. (b) Carotid artery angiography during stent implantation. (c) The balloon catheter was inflated to 7–9 atm to deploy the stent; red arrow indicates the balloon catheter in the right carotid artery. (d) Corroded iron stent was implanted into the right carotid artery; red arrow indicates position of the stent implanted into carotid artery. (e–f) HE staining showed that the intimal thickness was lower in the corroded iron stent-implanted group. Yellow dashed lines demarcate the intimal hyperplasia after stenting. (g–h) Percentage of VSMCs in the S phase were reduced in corroded iron stent group (flow cytometry) (i) Numerous corroded granules were produced around the struts on month 6 after the iron stent implantation (the right one). However, few corroded granules could be found on month 1 (the left one). The green arrow indicates the corroded granules accumulated around the struts of the iron stent. (j–k) Both OPN and α-SMA were decreased on month 6. Bars represent mean ± SD. *P < 0.05; **P < 0.01. (For interpretation of the references to colour in this figure legend, the reader is referred to the Web version of this article.)

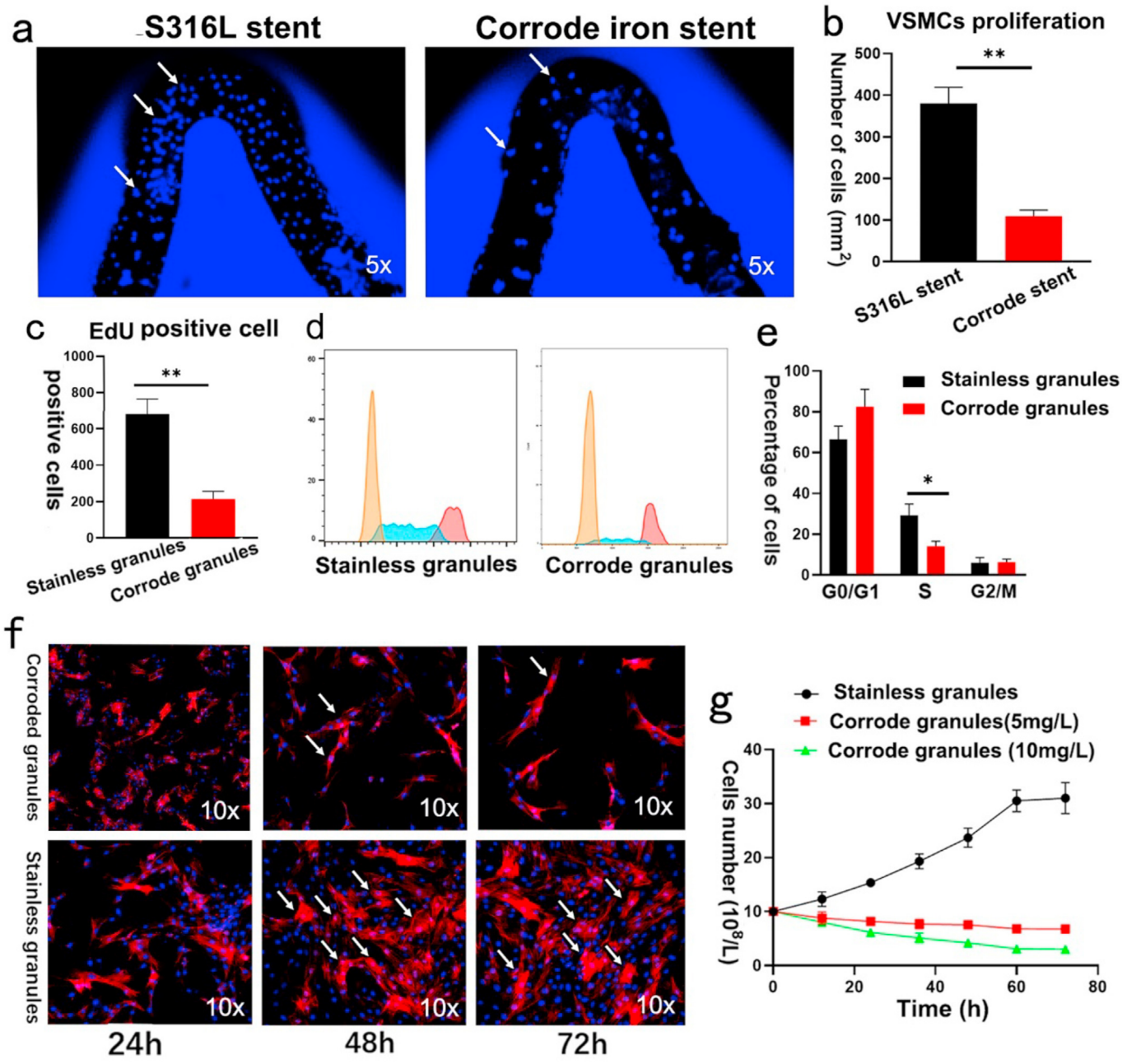

Fig. 3. Corroded granules inhibited VSMC proliferation *in vitro*. (a–b) VSMC proliferation was reduced on surface of the corroded iron stent. White arrows indicate VSMC. (c) Numbers of EdU-positive cells were decreased when pretreated with corroded granules. (d–e) Corroded granules decreased the percentage of VSMCs in the S phase (flow cytometry). (f–g) Corroded granules attenuated VSMC proliferation in a dose-dependent manner. White arrows indicate VSMCs. Bars represent mean ± SD. *P < 0.05; **P < 0.01.

the number of EdU-positive cells in the control group (Fig. 4h). Similar results were obtained from *in vivo* experiments. The iron stent-implanted group exhibited increased AMPK expression and mTOR downregulation compared to that of the S316L stent-implanted group (Fig. 4i). Collectively, these data revealed that corroded granules stimulated autophagy to inhibit VSMC proliferation via the AMPK/mTOR pathway.

3.6. Corroded iron stent inhibits VSMC proliferation in atherosclerotic stenosis

VSMC proliferation was a key mechanism in restenosis. Thus, we introduced the corroded iron stent to evaluate the effect of iron corroded granules on VSMC proliferation in atherosclerotic artery stenosis, and a balloon-induced intimal injury atherosclerotic stenosis model was introduced for the study. Atherosclerotic stenosis was induced in the carotid artery by a high-lipid diet, following balloon catheter injury to the endothelium. Angiographic analyses were performed to verify artery stenosis. All rabbits (n = 14; weight 5.5 kg ± 0.5 kg) were successfully stented, 6 month was set as the time point to evaluate the results. No periprocedural complications occurred during the experiment period. As shown in Fig. 5a, the cross-sectional area of the carotid artery decreased after balloon injury-associated high-cholesterol feeding. Strikingly, the stenosis segment re-expanded after deploying the corroded iron stent (Fig. 5b), indicating a satisfactory mechanism support in atherosclerotic stenosis. In addition, we found that the intimal thickness was lower in the corroded iron stent-implanted group (Fig. 5c–d). Likewise, the intima/

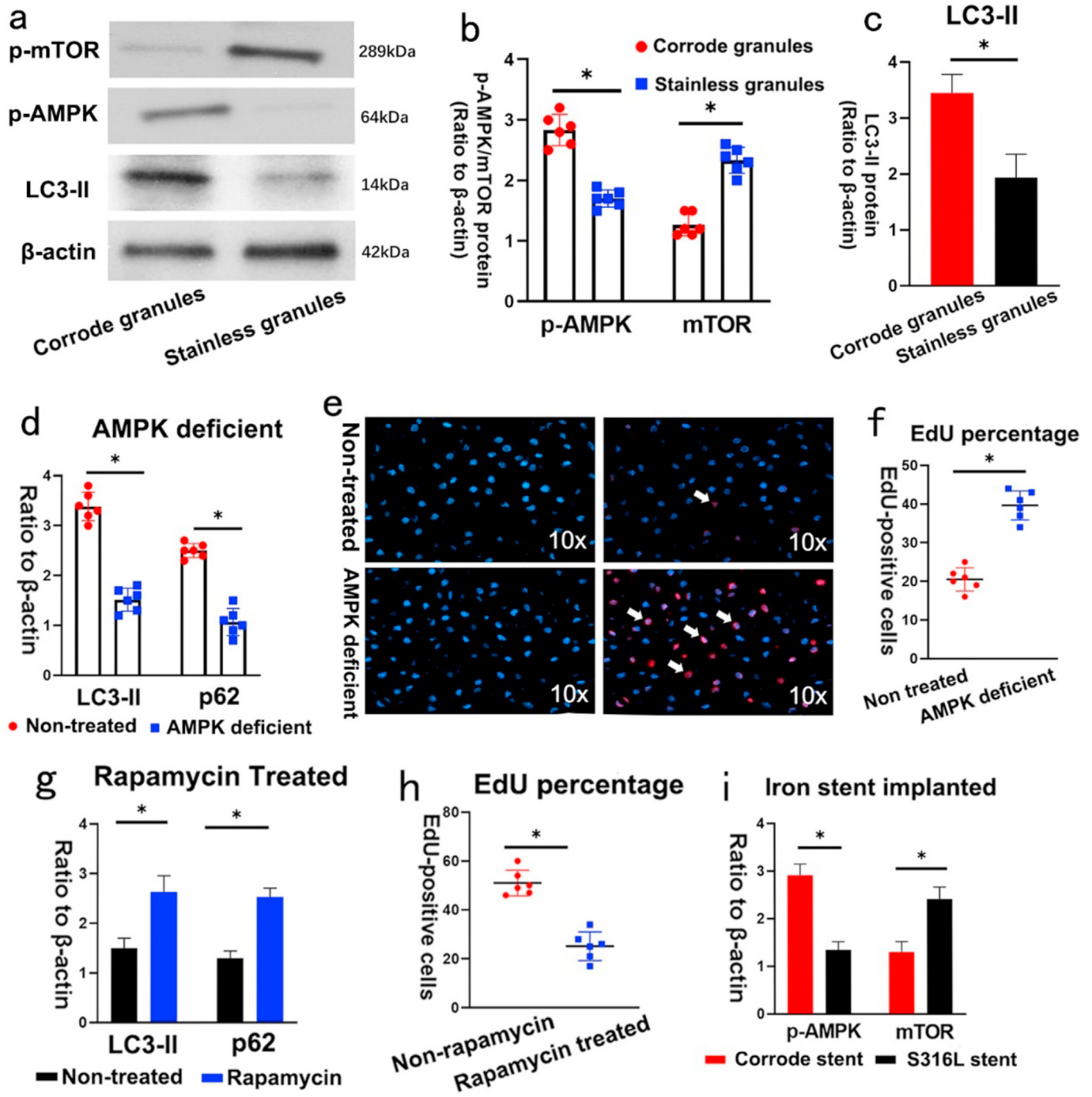

Fig. 4. Corroded granules activated autophagy through AMPK/mTOR signaling pathway. (a–c) Phosphorylation of AMPK (p-AMPK) and the protein level of LC3-II were increased in corroded granules group, whereas the phosphorylation of mTOR (p-mTOR) was reduced. (d) LC3-II and p62 expression induced by corroded granules were decreased in AMPK-deficient VSMC. (e–f) EdU-positive cells were remarkably increased in AMPK-deficient VSMC. The white arrow indicates EdU-positive cells. (g) Decreased protein expression of p62 and LC3-III were elevated in stainless granules group after introducing the rapamycin. (h) Rapamycin pre-treatment significantly reduced the number of EdU-positive cells in stainless granules group. (i) Corrode iron stent implanted group exhibited increased AMPK expression and mTOR down-regulation compared to that of S316L stent group. Bars represent mean ± SD. *P < 0.05.

media (I/M) ratio also decreased (Fig. 5e), and α-SMA expression was attenuated in the intima layer (Fig. 5f). Flow cytometry analysis indicated that the percentage of VSMC in the S phase was reduced, indicating a low proliferation rate after the implantation of the corroded iron stent (Fig. 5g). To investigate autophagy activity in atherosclerotic stenosis areas, the expression of p62 protein and LC3-II was measured in this study. Intriguingly, the p62 protein and LC3-II levels were higher in the iron stent group (Fig. 5h). Consistent with the elevated levels of p62 and LC3-II, autophagosome formation was found to increase after implanting the corroded iron stent (Fig. 5i). However, after pre-treatment with the autophagy inhibitor 3-MA, the number of autophagosomes was reduced in the corroded iron stent-implanted group (Fig. S4g), and p62 and LC3-II expression was also decreased (Fig. 5j). Intriguingly, no differences were identified in the intimal thickness between the corroded iron stent-implanted group and the S316L stent-implanted group (Fig. 5k). Taken together, these findings indicate that the corrode granules produced by

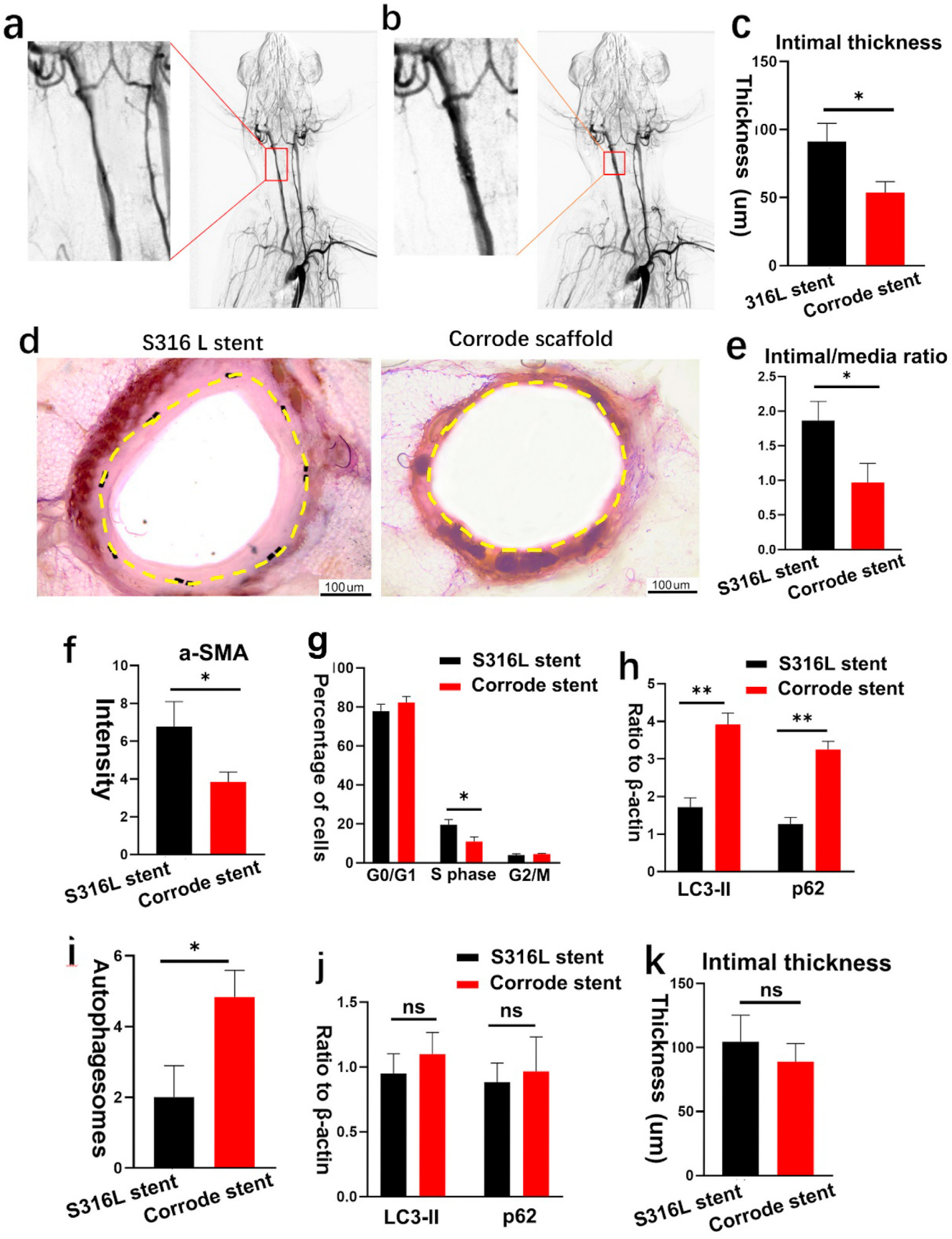

(caption on next page)

Fig. 5. Corroded iron stents inhibit VSMC proliferation in atherosclerotic stenosis. (a) Atherosclerotic stenosis was induced in right carotid artery by high lipid diet following balloon catheter injury to the endothelium. The cross-section area was decreased in carotid artery after balloon-injury-associated high cholesterol feeding. (b) The stenosis segment was re-expanded after deploying corroded iron stent. All rabbits (n = 14; weight 5.5 kg ± 0.5 kg) were successfully stented , and were remained healthy until the final follow up. (c–d) Intimal thickness was lower in corroded stent-implanted group. Yellow dashed lines demarcate the intimal hyperplasia after stenting. (e) Intima/media (I/M) ratio was decreased in corroded stent-implanted group. (f) α-SMA expression was attenuated in intima layer in corroded stent-implanted group. (g) Flow cytometry analysis indicated that the percentage of VSMC in the S phase were reduced in corroded iron stent-implanted group. (h) Expression of p62 protein and LC3-II were increased in corroded iron stent-implanted group. (i) Autophagosomes formation was increased after deploying the corroded stent. (j) Expression of p62 protein and LC3-II were decreased after pre-treatment with the autophagy inhibitor 3-MA. (k) No statistical differences were identified in intimal thickness between the two groups after pre-treatment with the autophagy inhibitor 3-MA. Bars represent mean ± SD. *P < 0.05; **P < 0.01. (For interpretation of the references to colour in this figure legend, the reader is referred to the Web version of this article.)

iron stents prevent VSMC proliferation in atherosclerotic stenosis via activating autophagy.

3.7. Corroded granules prevent inflammatory response in atherosclerotic stenosis

Inflammatory mediators in atherosclerotic stenosis are essential for stimulating VSMC proliferation after stenting. However, whether inflammatory cytokines are activated in response to the corroded stent is unclear. To address this question, we investigated systemic inflammatory cytokines after implanting the corroded iron stent. Remarkably, compared with the S316L stent group, the levels of C-reactive protein, TNF-α, and IL-6 were decreased in the iron-corroded stent-implanted group (Fig. 6a). Conversely, the expression of TGF-β and IL-10 was increased (Fig. 6b). However, no differences were identified in IL-1, IL-8, and IL-12 levels between the groups (Fig. 6c). The development of atherosclerotic restenosis involves complex patterns of interaction between inflammatory cells and VSMC proliferation. Thus, inflammatory cells were associated with neoatherosclerosis and restenosis after the stent was implanted. Therefore, we further measured inflammatory cell infiltration. Consistent with the decrease in proinflammatory cytokines, the percentage of neutrophil granulocytes ($CD45^+CD11b^+Ly6G^+$) was reduced in the corroded iron stent-implanted group (Fig. 6d–e). However, the percentage of Tregs ($CD4^+CD25^+Foxp3^+$) was increased (Fig. 6f). Notably, no significant differences were identified in M1 ($F4/80^+CD11b^+CD86^+$) or M2 ($F4/80^+CD11b^+CD206^+$) between the groups. These findings demonstrate that the inflammatory response in atherosclerotic stenosis was attenuated by the iron-corroded stent.

3.8. Hemocompatibility evaluation of iron corroded granules

Corroded granules may be carried away by the blood and block downstream distal branches. Thus, the risk of thrombosis after iron stent implantation needs to be evaluated, and follow-up angiography was performed in the study. As shown in Figs. S3a–c, no occlusion was found in the distal branch of the iliac or intracranial arteries. Moreover, no abnormalities were detected in the histomorphological observations of the liver, kidneys, and lungs (Fig. S3d). The corroded granules could possibly be degraded and release iron ions into the blood, which may increase the concentration of serum iron ions and lead to heavy metal intoxication. Therefore, we measured the levels of serum iron ions after stent implantation. As shown in Table 1, the iron ion levels were normal, and no statistical differences were found between the corroded iron stent and S316L stent. Platelets are critical for restenosis after stenting, and we measured platelet adhesion and activation on the corroded iron stent. As shown in Fig. S3e, although numerous corrosion pits were produced on the iron stent, almost all the platelets that adhered to the surface remained round and showed no sign of pseudopodia-like structures, indicating negative activation in the corroded iron stent. The PT and APTT tests were used to evaluate the activation of coagulation factors. To assess the effect of the corroded granules on coagulation factors, the bioactivity of the coagulation factor was investigated further. As shown in Fig. S3 f-g, the PT and APTT of the iron stent were almost the same as those of the S316L stent group, indicating that the corroded granules did not activate coagulation factors. Hemolysis ratio is critical to evaluate the hemocompatibility of blood-contacting materials. Thus, we evaluated the hemolysis ratio. As presented in Fig. S4d, the hemolysis performance of corroded iron stent and S316L stent were 0.59 ± 0.18% and 0.61 ± 0.17%, respectively, which was much lower than 5%, a judging criterion for excellent blood compatibility according to ISO 10993–4. As the iron stent corrosion changed the topography and chemistry in its surface, and it is important to evaluate if these changes induced any toxicity to the cells. Thus, cytotoxicity of corroded iron stent was measured using the lactate dehydrogenase (LDH) assay. The result showed that corroded iron stent had the similar amount of LDH expression compared to the positive control (100% live cells), indicating neither the corroded iron stent nor S316L stent induced cytotoxic effects (Fig. S4e). The complement system plays an important role in the body's defense mechanism against foreign invaders. Complement is activated by plasmin through the cleavage of C3 into C3a and C3b. Therefore, we measured the concentration of C3a in serum after incubating with corroded iron stent and the S316L stent. As exhibited in Fig. S4f, despite the C3a concentration was slightly higher in corroded iron stent. However, no statistic differences were identified between the two groups. Taken together, these data reveal that the corroded iron stent had satisfactory hemocompatibility after implantation.

4. Discussion

With the advent of DES, the incidence of neointimal hyperplasia has decreased because of the suppression of VSMCs. Although the risk of in-stent restenosis was reduced with DES, it prevented the re-endothelialization process [26–28]. Therefore, the beneficial effects of DES are at the cost of inhibiting neo-endothelial formation, which is closely related to late and very late in-stent thrombosis. Thus, stents that specifically target VSMCs but not the endothelium constitute the next revolution in interventional technology. Bioresorbable stents were heralded as the fourth revolution in stents and were designed to avoid the shortcomings posed by DES [29,30]. Iron and iron alloys are candidate materials for bioresorbable stents because of their excellent mechanical performance and biocompatibility [12,13,24]. Notably, the incidence of intimal hyperplasia was previously demonstrated to be much lower in nitrided iron-based stents than in S316L stents. We hypothesized that the corroded granules produced by the iron stent prevented intimal hyperplasia by inhibiting VSMCs, as VSMC proliferation is one of the leading causes of intimal hyperplasia.

To verify this hypothesis, we implanted the corroded stent into the artery, we found that it attenuated VSMC proliferation, which inhibited neointimal hyperplasia after stenting. This finding was further confirmed *in vitro* in co-culture experiments. We also evaluated the safety and biocompatibility of corroded granules after iron stent implantation. Taken together, these results provide insights into iron-corroded granules and a new framework for preventing neointimal hyperplasia after stenting.

Iron is an essential element involved in diverse physiological processes, including DNA synthesis and oxygen binding [15,16]. Iron plays a beneficial role in intimal hyperplasia by antagonizing VSMC proliferation. In addition, in the presence of excess Fe (II), VSMC were mostly retained in the quiescent and no proliferative G_0 phase. These findings imply that increased iron inhibits VSMC proliferation. However, this

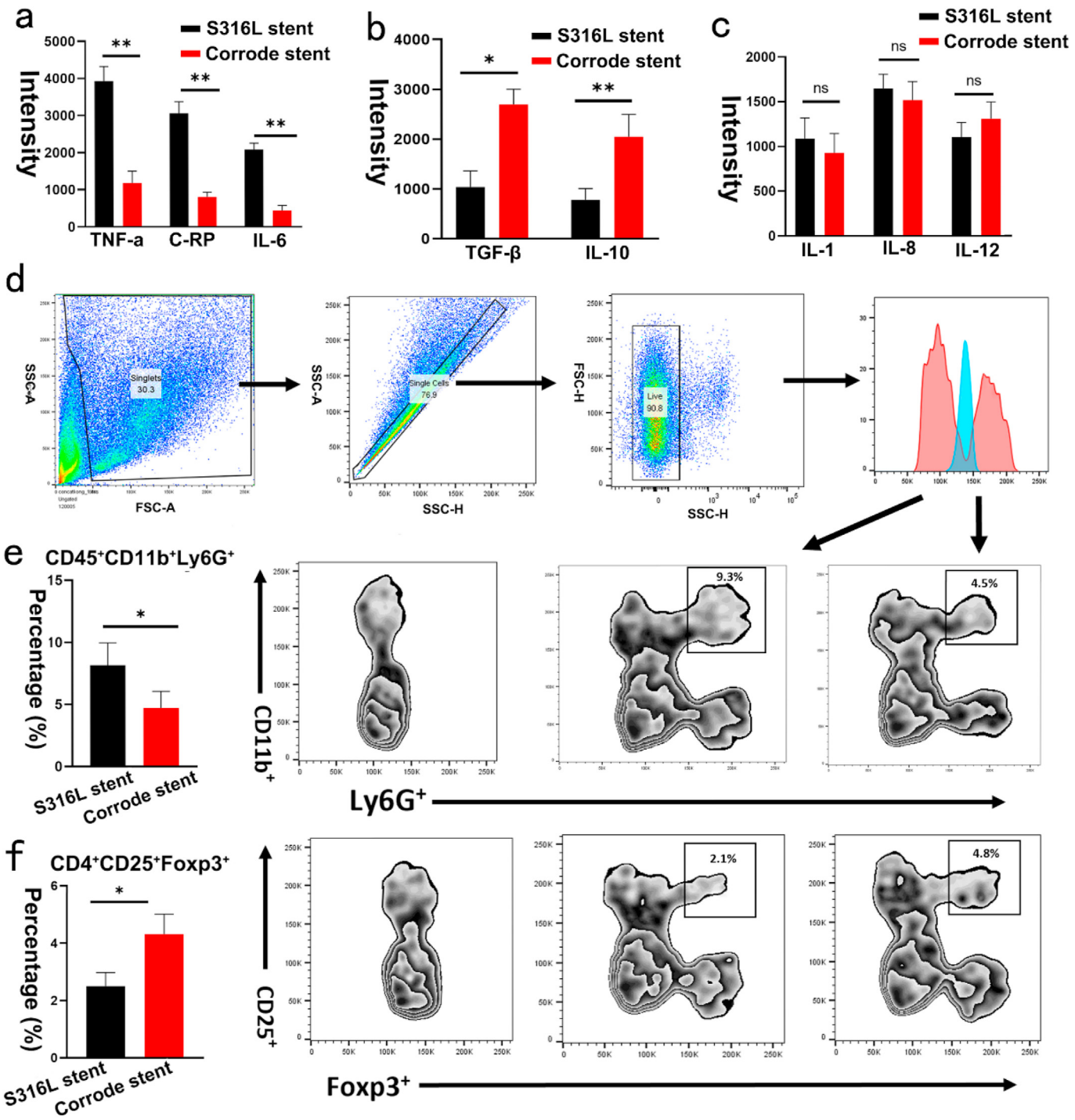

Fig. 6. Corroded iron stents prevent inflammatory response in atherosclerotic stenosis. (a) Levels of C-reactive protein, TNF-α, and IL-6 were decreased in iron corroded stent-implanted group. (b) Expression of IL-10 and TGF-β were increased in iron corroded stent-implanted group. (c) No statistical differences were identified in IL-1, IL-8, and IL-12 between the iron corroded stent-implanted group and the S316L stent implanted group. (d) Gating strategies used for measurement of neutrophils ($CD45^+$ $CD11b^+$ $Ly6G^+$). (e) Percentage of neutrophil granulocytes ($CD45^+CD11b^+Ly6G^+$) was reduced in iron corroded stent-implanted group. (f) Percentage of Tregs ($CD4^+CD25^+Foxp3^+$) were increased in iron corroded stent-implanted group. Bars represent mean ± SD. *P < 0.05; **P < 0.01.

potentially beneficial effect has only been demonstrated *in vitro* and requires further validation in animal models. Therefore, we implanted a corroded iron stent into the rabbit to study the role of the corroded granules on VSMC using the S316L stent as the control. We found that the expression of OPN, a biomarker of the synthetic phenotype, was greatly decreased in the corroded stent group. In addition, the percentage of VSMC in the S phase was reduced in the corroded stent group. These findings suggest that VSMC proliferation was attenuated by the production of corroded granules. In addition to VSMC, neointimal hyperplasia was measured after iron stent implantation. Notably, we found that the intimal thickness was much lower in the corroded stent group and that the intima/media (I/M) ratio also decreased. Based on these findings, we concluded that the corroded granules produced by the iron stent inhibited VSMC proliferation, which consequently attenuated neointimal hyperplasia after stenting.

In physiological conditions, VSMCs are in a quiescent state

Table 1
Level of serum iron ions after stenting.

Animal ID	Group	
	S316L Stent (*umol/L*)	Corroded Stent (*umol/L*)
1	***67.4***	***75.9***
2	***75.9***	***65.4***
3	***65.3***	***77.7***
4	***71.4***	***69.3***
5	***82.1***	***86.4***
6	***78.3***	***79.5***
7	***68.7***	***76.3***
P*		***0.3979***

*$P < 0.05$, considered statistically significant.

characterized by a low rate of cell replication. However, once stimulated by intimal injury or inflammatory remodeling, the quiescent VSMCs demonstrated to shift from a contractile phenotype in media layer toward a synthetic state into the intima layer. The synthetic phenotype of VSMCs is characterized by proliferation and migration. OPN demonstrated to be one of marker in VSMCs synthetic phenotype. As in this study, the expression of OPN was reduced in corroded iron stent group, indicating the percentage of synthetic phenotype decreased after the iron stent corroded. In addition to the OPN, S100A4 demonstrated to be the reliable marker of synthetic phenotype VSMCs by inhibiting phosphorylation of target proteins. Then we also measured the expression of S100A4 between corroded iron stent group and the control. In consistent with the results of OPN, the expression of S100A4 was decreased in corroded iron stent group. Based on those results, we indicated that the percentage of VSMCs in synthetic phenotype was decreased after iron stent corrosion.

The effects of the corroded granules on the VSMC were further validated according to the corroded phase after iron stent implantation. Because corroded granules were generated several days after implantation, no observable effect occurred in the initial stages. Next, we assessed the biological characteristics of VSMCs during the initial and later periods after stenting. As expected, a few corroded granules were observed in the media layer in the initial state, and their levels increased significantly in the later period. In line with the accumulation of corroded granules, OPN and α-SMA expression also decreased in the later stages. These findings are consistent with the results obtained from the animal model presented above, further confirming that corroded granules inhibit VSMC proliferation after iron stent implantation.

Local hemodynamic factors, including wall shear stress and blood flow velocity, influence VSMC proliferation [31,32]. Mechanical stretching caused by hemodynamic conditions promotes VSMC proliferation by activating the PI3K/Akt, MAPK, and RhoA/Rho kinase pathways [33,34]. The surface of the corroded iron stent became rough and uneven at the sites of the corroded pits. Thus, hemodynamic conditions may change owing to the mechanical structure generated by the corroded pits. Therefore, the hemodynamic conditions between the corroded stent and control stent must be navigated. The mechanical performance of stents with different designs can be studied by computational analysis using finite element analysis to assess the hemodynamic conditions among the groups. Remarkably, although the corroded pits covered the surface of the iron stent, no significant differences in wall shear stress were detected between the corroded stent and control stent. This result indicates that corrosion in the stent had minimal influence on the wall shear stress. In addition to wall shear stress, the blood flow velocity was almost the same between the two groups. Based on these results, the influence of hemodynamic conditions on VSMC could be ruled out.

Autophagy is an important biological process involved in cellular homeostasis [35–37]. Notably, autophagy was involved in regulating VSMC proliferation, migration, and collagen secretion in response to stimuli [36,38]. Here, we showed that corroded granules inhibited VSMC proliferation by activating autophagy. In line with our findings, similar studies have showed that the activation of autophagy inhibited the VSMC proliferation. For instance, Cho et al. indicated that indatraline induces autophagy and prevents VSMC proliferation by inhibiting the mTOR/S6 kinase signaling pathway [39]. Zheng et al. reported that Nkx2-3 inhibits VSMC proliferation by promoting autophagy through the AMPK/mTOR signaling pathway [40]. In addition, inhibition of autophagy in VSMC results in p16-mediated G_1-cell cycle arrest and promotes collagen secretion [41]. These observations, together with our findings, suggest that autophagy plays an important role in restenosis by regulating VSMC proliferation. However, some studies have shown that autophagy has the opposite effect on VSMC proliferation. For example, pre-treatment of VSMCs with the secreted protein sonic hedgehog promoted autophagy and led to an increase in VSMC proliferation [42]. The reason for this disparity in VSMC responses to autophagy could be as follows: uncertainty exists regarding the cell signaling pathways, stimulation type, and transcriptional processes that were varied to induce VSMC proliferation in response to different stimuli. Additionally, autophagy is much more complex, involving lysosomal degradation of extracellular material, plasma membrane proteins, and cytosolic components. Therefore, the effects of autophagy on VSMC function could be multifactorial. Thus, further studies are required to elucidate the mechanism through which autophagy regulates VSMC proliferation via corroded granules.

Previously, the AMPK/mTOR signaling pathway was found to be a major regulator of autophagy. Notably, AMPK activation inhibited VSMC proliferation and prevented vascular intimal hyperplasia. In contrast, mTOR negatively regulates autophagy by phosphorylating Atg1/unc-51 like autophagy activating kinase 1 (ULK1) [43]. In addition, activation of the AMPK/mTOR signaling pathway upregulated autophagy to restrain VSMC proliferation in balloon-injured arteries [39,44]. Thus, we speculated that corroded granules might induce autophagy by activating the AMPK/mTOR signaling pathway. By detecting the expression of AMPK/mTOR-related proteins both *in vivo* and *in vitro*, we revealed that the phosphorylation of AMPK (p-AMPK) and the protein level of LC3 II were increased in the corroded granule group, whereas p-mTOR was reduced. Moreover, the number of EdU-positive cells was markedly increased in AMPK-deficient VSMC. To clarify the role of mTOR in autophagy activation, we introduced rapamycin to inhibit the mammalian target of rapamycin pathway. Rapamycin pre-treatment significantly reduced the number of EdU-positive cells in the control group. Additionally, the decreased protein expression of p62 and LC3-II/I were elevated in this group. Taken together, this data proves that corroded granules enhance autophagy via the AMPK/mTOR pathway and inhibit VSMC proliferation; to our knowledge, this is the first work that proves this relationship. Therefore, targeting mTOR and/or AMPK may provide effective strategies to prevent vascular remodeling and restenosis after stenting.

It should be mention that iron stent corrosion could influenced the Fe ion release and the PH, which might also influence the cells behavior in the study. We intended to set the new iron stent as the control at the beginning. However, the new iron stent could be corroded after implantation, and it had the similar effects of corroded iron stent on surrounding cells. Therefore, we just set the S316L stent as the control, and the effects of Fe ion releasing as well as the PH on VSMCs proliferation cannot be ruled out from the study currently.

5. Conclusions

Neointimal hyperplasia induced by VSMC proliferation is a major cause of restenosis. Thus, inhibiting VSMC proliferation is critical for preventing in-stent restenosis. In this study, we demonstrated that iron stent produced the corroded granules after implantation, and the main component of the corrosion granules was iron oxide. In addition, the corroded iron stent reduced the neointimal hyperplasia in an atherosclerotic stenosis model. Moreover, corroded granules decreased the neointimal hyperplasia by inhibiting VSMC proliferation. We also revealed that corroded granules reduced VSMC proliferation by activating autophagy through the AMPK/mTOR signaling pathway. Importantly, the safety of iron corroded granules was evaluated and proved to

be satisfactory hemocompatibility in rabbit model. Overall, the role of corroded granules in restenosis prevention was described for the first time. These findings provide insights into the role of iron-corroded granules in inhibiting VSMC proliferation, pointing to a new direction to prevent restenosis after stenting.

Author contributions

D.Q drafting the manuscript; D.Q and Y.D performed the research; J.X and C.C designed the study; Y.W, J.Y, G.Z and J.F supervised the study; D.Q, Y.D, M.S and J.H analyzed the data; J.X and C.C revised the final version of the manuscript.

Declaration of competing interest

The authors declare that they have no known competing financial interests or personal relationships that could have appeared to influence the work reported in this paper.

Acknowledgements

This work was supported by the National Natural Science Foundation of China (Nos. 81974223 and 81271325).

Appendix A. Supplementary data

Supplementary data to this article can be found online at https://doi.org/10.1016/j.mtbio.2022.100420.

References

[1] S.F. Braga, J.R. Neves, J. Ferreira, C. Carrilho, J.C. Simoes, A. Mesquita, Neointimal hyperplasia, Rev. Port. Cir. Cardiotorac. Vasc. 26 (2019) 213–217.
[2] V. Sorokin, K. Vickneson, T. Kofidis, et al., Role of vascular smooth muscle cell plasticity and interactions in vessel wall inflammation, Front. Immunol. 11 (2020), 599415.
[3] G. Wang, L. Jacquet, E. Karamariti, Q. Xu, Origin and differentiation of vascular smooth muscle cells, J. Physiol. 593 (2015) 3013–3030.
[4] A. Curcio, D. Torella, C. Indolfi, Mechanisms of smooth muscle cell proliferation and endothelial regeneration after vascular injury and stenting: approach to therapy, Circ. J. 75 (2011) 1287–1296.
[5] C.J. Lin, B.M. Hunkins, R.A. Roth, C.Y. Lin, J.E. Wagenseil, R.P. Mecham, Vascular smooth muscle cell subpopulations and neointimal formation in mouse models of elastin insufficiency, Arterioscler. Thromb. Vasc. Biol. 41 (2021) 2890–2905.
[6] E. Im, M.K. Hong, Drug-eluting stents to prevent stent thrombosis and restenosis, Expert Rev. Cardiovasc Ther. 14 (2016) 87–104.
[7] I. Rykowska, I. Nowak, R. Nowak, Drug-eluting stents and balloons-materials, structure designs, and coating techniques: a review, Molecules 25 (2020).
[8] O. Ben-Yehuda, Long-term outcomes with drug-eluting stents: beyond stent choice, J. Am. Coll. Cardiol. 76 (2020) 159–161.
[9] A. Kastrati, S. Kufner, Progress in drug-eluting stent technology: have we come to the end of the road? JACC Cardiovasc. Interv. 12 (2019) 1661–1664.
[10] D. Regazzoli, P.P. Leone, A. Colombo, A. Latib, New generation bioresorbable scaffold technologies: an update on novel devices and clinical results, J. Thorac. Dis. 9 (2017) S979–S985.
[11] Y. Sotomi, Y. Onuma, C. Collet, et al., Bioresorbable scaffold: the emerging reality and future directions, Circ. Res. 120 (2017) 1341–1352.
[12] W. Lin, L. Qin, H. Qi, et al., Long-term in vivo corrosion behavior, biocompatibility and bioresorption mechanism of a bioresorbable nitrided iron scaffold, Acta Biomater. 54 (2017) 454–468.
[13] G. Sun, W. Guo, H. Zhang, X. Ma, X. Jia, J. Xiong, A novel iron-bioresorbable sirolimus-eluting scaffold device for infrapopliteal artery disease, JACC Cardiovasc. Interv. 15 (2022) e57–e59.
[14] J.F. Zheng, H. Qiu, Y. Tian, et al., Preclinical evaluation of a novel sirolimus-eluting iron bioresorbable coronary scaffold in porcine coronary artery at 6 months, JACC Cardiovasc. Interv. 12 (2019) 245–255.
[15] R. Evstatiev, C. Gasche, Iron sensing and signalling, Gut 61 (2012) 933–952.
[16] T. Kondori, T.N. Akbarzadeh, H. Ghaznavi, et al., A binuclear iron(III) complex of 5,5'-dimethyl-2,2'-bipyridine as cytotoxic agent, Biometals 33 (2020) 365–378.
[17] F. Thevenod, Iron and its role in cancer defense: a double-edged sword, Met. Ions Life Sci. 18 (2018).
[18] P.P. Mueller, T. May, A. Perz, H. Hauser, M. Peuster, Control of smooth muscle cell proliferation by ferrous iron, Biomaterials 27 (2006) 2193–2200.
[19] E. Scarcello, A. Herpain, M. Tomatis, F. Turci, P.J. Jacques, D. Lison, Hydroxyl radicals and oxidative stress: the dark side of Fe corrosion, Colloids Surf. B Biointerfaces 185 (2020), 110542.
[20] M. Schinhammer, I. Gerber, A.C. Hanzi, P.J. Uggowitzer, On the cytocompatibility of biodegradable Fe-based alloys, Mater. Sci. Eng. C Mater. Biol. Appl. 33 (2013) 782–789.
[21] W. Durante, Heme oxygenase-1 in growth control and its clinical application to vascular disease, J. Cell. Physiol. 195 (2003) 373–382.
[22] X.M. Liu, G.B. Chapman, H. Wang, W. Durante, Adenovirus-mediated heme oxygenase-1 gene expression stimulates apoptosis in vascular smooth muscle cells, Circulation 105 (2002) 79–84.
[23] K.J. Peyton, S.V. Reyna, G.B. Chapman, et al., Heme oxygenase-1-derived carbon monoxide is an autocrine inhibitor of vascular smooth muscle cell growth, Blood 99 (2002) 4443–4448.
[24] W. Lin, H. Zhang, W. Zhang, et al., In vivo degradation and endothelialization of an iron bioresorbable scaffold, Bioact. Mater. 6 (2021) 1028–1039.
[25] W. Lin, G. Zhang, P. Cao, et al., Cytotoxicity and its test methodology for a bioabsorbable nitrided iron stent, J. Biomed. Mater. Res. B Appl. Biomater. 103 (2015) 764–776.
[26] J. Aoki, K. Tanabe, Mechanisms of drug-eluting stent restenosis, Cardiovasc. Interv. Ther. 36 (2021) 23–29.
[27] G. Katz, B. Harchandani, B. Shah, Drug-eluting stents: the past, present, and future, Curr. Atherosclerosis Rep. 17 (2015) 485.
[28] E. Shlofmitz, M. Iantorno, R. Waksman, Restenosis of Drug-Eluting Stents: A New Classification System Based on Disease Mechanism to Guide Treatment and State-Of-The-Art Review, vol. 12, Circ Cardiovasc Interv, 2019, e007023.
[29] B. Forrestal, B.C. Case, C. Yerasi, A. Musallam, C. Chezar-Azerrad, R. Waksman, Bioresorbable scaffolds: current technology and future perspectives, Rambam Maimonides Med. J. 11 (2020).
[30] X. Peng, W. Qu, Y. Jia, Y. Wang, B. Yu, J. Tian, Bioresorbable scaffolds: contemporary status and future directions, Front Cardiovasc. Med. 7 (2020), 589571.
[31] N.C.A. van Engeland, A. Pollet, J.M.J. den Toonder, C.V.C. Bouten, O. Stassen, C.M. Sahlgren, A biomimetic microfluidic model to study signalling between endothelial and vascular smooth muscle cells under hemodynamic conditions, Lab Chip 18 (2018) 1607–1620.
[32] H. Zhang, Z. Yang, J. Wang, X. Wang, Y. Zhao, F. Zhu, Wall shear stress promotes intimal hyperplasia through the paracrine H2O2-mediated NOX-AKT-SVV axis, Life Sci. 207 (2018) 61–71.
[33] C. Chaabane, F. Otsuka, R. Virmani, M.L. Bochaton-Piallat, Biological responses in stented arteries, Cardiovasc. Res. 99 (2013) 353–363.
[34] S. Tada, J.M. Tarbell, Interstitial flow through the internal elastic lamina affects shear stress on arterial smooth muscle cells, Am. J. Physiol. Heart Circ. Physiol. 278 (2000) H1589–H1597.
[35] E. Mameli, A. Martello, A. Caporali, Autophagy at the interface of endothelial cell homeostasis and vascular disease, FEBS J. 289 (2021) 2976–2991.
[36] J.K. Salabei, B.G. Hill, Autophagic regulation of smooth muscle cell biology, Redox Biol. 4 (2015) 97–103.
[37] G.R. De Meyer, M.O. Grootaert, C.F. Michiels, A. Kurdi, D.M. Schrijvers, W. Martinet, Autophagy in vascular disease, Circ. Res. 116 (2015) 468–479.
[38] J.K. Salabei, B.G. Hill, Implications of autophagy for vascular smooth muscle cell function and plasticity, Free Radic. Biol. Med. 65 (2013) 693–703.
[39] Y.S. Cho, C.N. Yen, J.S. Shim, et al., Antidepressant indatraline induces autophagy and inhibits restenosis via suppression of mTOR/S6 kinase signaling pathway, Sci. Rep. 6 (2016), 34655.
[40] H. Zheng, W. Zhai, C. Zhong, et al., Nkx2-3 induces autophagy inhibiting proliferation and migration of vascular smooth muscle cells via AMPK/mTOR signaling pathway, J. Cell. Physiol. 236 (2021) 7342–7355.
[41] S. Tai, X.Q. Hu, D.Q. Peng, S.H. Zhou, X.L. Zheng, The roles of autophagy in vascular smooth muscle cells, Int. J. Cardiol. 211 (2016) 1–6.
[42] H. Li, J. Li, Y. Li, et al., Sonic hedgehog promotes autophagy of vascular smooth muscle cells, Am. J. Physiol. Heart Circ. Physiol. 303 (2012). .H1319-1331.
[43] S. Alers, A.S. Loffler, S. Wesselborg, B. Stork, Role of AMPK-mTOR-Ulk1/2 in the regulation of autophagy: cross talk, shortcuts, and feedbacks, Mol. Cell Biol. 32 (2012) 2–11.
[44] H. Wu, A. Song, W. Hu, M. Dai, The anti-atherosclerotic effect of paeonol against vascular smooth muscle cell proliferation by up-regulation of autophagy via the AMPK/mTOR signaling pathway, Front. Pharmacol. 8 (2017) 948.